MASTER'S THESIS:

HYDROTHERMAL SYNTHESIS PROCESS FOR THE PRODUCTION OF SILICALITE-1 CRYSTAL AGGREGATE PACKING PARTICLES

A Thesis Submitted in Partial Fulfillment of the Requirements
For the Degree of Master of Science in Chemical Engineering
at Worcester Polytechnic Institute
February 2010

Submitted By:

BRADFORD J. CARLEEN
WORCESTER POLYTECHNIC INSTITUTE
WORCESTER, MA 01609

Date: 14 January 2010

Submitted To:

Dr. Robert Thompson, Advisor

Dr. David DiBiasio, Department Head
Chemical Engineering

ABSTRACT

Methyl Tertiary-Butyl Ether (MTBE) contamination of groundwater and surface waters has become a relevant environmental and public safety concern in recent years. This anthropogenic compound is now persistent at low concentrations in several valuable ground and surface water locations within the United States due largely to the widespread production of MTBE for use as a fuel oxygenate in conjunction with negligent underground storage practices during the 1980's and 1990's. Though there are several treatment strategies for the remediation of MTBE spill sites, the most efficient strategy may be adsorption of MTBE by a packed column of silicalite-1 adsorbent. Effective adaption of this technology requires cheap production of silicalite-1 sorbent packing particles on the order of 3 millimeters diameter. This work entails the development of a new synthesis process which results in sufficient in-situ crystallization of silicalite-1 aggregates within a 3 millimeter spherical amorphous silica gel source. The crystal aggregates sizes can be tuned from 5 to 70 μm, depending on synthesis parameters, and the finished silicalite-1 aggregate particle takes the shape of the amorphous gel source. These aggregate particles, when containing a small amorphous core, should be suitable for packed adsorption column applications.

Multiple hydrothermal synthesis experiments were performed by batch methods featuring silica gel spheres as the sole silica source for the batch. Zeolite nucleation and crystal growth were demonstrated throughout the amorphous bead. Synthesis parameters were optimized both for short synthesis times, optimal mechanical properties, and cost effectiveness. The influence of product crystal size on particle hardness was also investigated. The packing production process is sufficiently ready for supporting pilot scale adsorption studies.

ACKNOWLEDGEMENTS

I would like to thank my advisor Professor Robert W. Thompson for his direction and guidance throughout this work. It was my great honor to have had the opportunity to learn from one of the most noted experts in the field of microporous and mesoporous materials.

I would like to thank the Worcester Polytechnic Institute Chemical Engineering Department as a whole for all of the support necessary for this project. I am thankful for the opportunity to have been a part of one of the best education and research teams in the country. It was my great privilege to work with the well-maintained panoply of material science equipment the department has at its disposal. Specific gratitude is in order for the work of: Doug White in keeping the x-ray diffractometer (XRD) and the scanning electron microscope (SEM) in perfect working order, a difficult task considering the age of this remarkable equipment; Jack Ferraro in the creating of the TEFLON-lined, stainless steel autoclaves that provided for a wealth of simultaneous experiments as well as for assistance with equipment located at Goddard Hall; Dr. Engin Ayturk for his training on the XRD and the SEM; Professor Boquan Li for assistance with equipment located at Washburn Shops as well as initial SEM and Vicker's Hardness training; and Pranoti Navare for assistance with the XRD at the WPI Gateway Research Center.

I would like to thank and acknowledge Sena Ada for her encouragement and the Mediterranean cooking which supported me throughout this entire project and throughout my career as a graduate student.

I also owe a great debt of gratitude to the DuPont Corporation for partial funding of this work.

TABLE OF CONTENTS

I. INTRODUCTION…… 1

II. EXPERIMENTAL……11

III. RESULTS AND DISCUSSION……15

IV.CONCLUSIONS……32

V. FUTURE WORK……33

VI. REFERENCES……34

LIST OF FIGURES

Figure 1: MFI pore structure and crystal habit……7

Figure 2: Silicalite-1 crystal aggregate shell with incomplete surface coverage at 30X magnification……16

Figure 3: Silicalite-1 crystal aggregates at 4000X magnification……..16

Figure 4: Low temperature crystal curve for silicalite-1……..17

Figure 5: Bead with a shell of silicalite-1 aggregates covering the surface……18

Figure 6: Intermediate temperature crystal curve for silicalite-1……..19

Figure 7: High temperature crystal curve for silicalite-1……..19

Figure 8: High Temperature silicalite-1 crystal curve additional data set……20

Figure 9: Typical silicalite-1 morphology x-ray powder diffraction pattern……20

Figure 10: Silicalite-1 x-ray diffraction pattern of a high temperature experiment demonstrating preferred orientations.……21

Figure 11: High Temperature Crystal Morphology……22

Figure 12: Low Silica:TPAOH crystallization curve……24

Figure 13: The silicalite-1 aggregate shell at low magnification……..26

Figure 14: The silicalite-1 aggregate shell at 500X……26

Figure 15: The silicalite-1 shell demonstrating thickness and curvature……27

Figure 16: A silicalite-1 shell with small crystal sizes and leaf-like morphology of aggregates……27

Figure 17: The amorphous core within the incompletely converted sphere, cleaved in half to demonstrate the absence of crystallization within……28

Figure 18: Vicker's Hardness testing of various crystal sizes of synthesisized silicalite-1 aggregate packing spheres……31

LIST OF TABLES

Table 1: List of Reagents……11

Table 2: Recipes for Silicalite-1 Batch Synthesis……13

Table 3: Low Silica:TPAOH experiments……24

Table 4: Comparison of geometrical parameters of silica gel conversion features……25

Table 5: Hypothesis testing performed on 3 level treatment experimentation results……29-30

I. INTRODUCTION

MTBE Contamination of Ground and Surface Waters in the United States

Methyl Tertiary-Butyl Ether (MTBE) contamination of groundwater and surface waters has become a relevant environmental and public safety concern in recent years. This anthropogenic compound is now persistent at low concentrations in several valuable ground and surface water locations within the United States, due largely to the widespread production of MTBE for use as a fuel oxygenate during the 1980's and 1990's. Underground storage of oxygenated fuel blends containing MTBE at gasoline dispensing facilities and industrial sites throughout the US without adequate erosion protection or leak detection methods and equipment are partly responsible for the current concentrations of MTBE in American groundwater near urban areas. Small concentrations of MTBE are readily detectable to human senses in potable water in the form of an unpleasant taste and odor. Furthermore, there is some evidence that suggests MTBE may be a chronic exposure carcinogen and strong evidence that MTBE is an acute exposure irritant to the nervous and respiratory systems at high vapor concentrations[1]. MTBE poses difficulty to environmental remediation schemes because of its high solubility, low adsorption affinity for soil, and high resistance to biodegradation. These characteristics lead to large plume sizes at point leaks and a tendency of the compound to defy the conventional passive natural attenuation techniques traditionally utilized in managing petroleum leaks and spills. Activated carbon adsorption is an acceptable treatment strategy, but activated carbon, like soil, has a somewhat low sorption capacity for MTBE when compared to microporous dealuminated zeolites, such as silicalite-1. Due to this fact, large crystal aggregates of silicalite-1, having approximately spherical shapes with 3 mm average diameter, are an extremely attractive alternative technology to activated carbon for full scale cleanups of petroleum spills and leaks where significant MTBE concentrations are present.

MTBE had been produced as early as 1979 in the United States for the purpose of increasing the octane number of petroleum fuels in order to reduce valve-seat wear in high compression-ratio internal combustion engines.[2] This relatively new fuel additive found increased demand in response to the phase-out of tetra-ethyl lead additives starting in 1973.[3] The Clean Air Act amendments passed in 1990 set a minimum oxygen content requirement of 2.7% by weight for fuels sold for use on United States roadways in urban areas during winter months in order to promote complete combustion in automobile engines and effectively reduce domestic mobile source carbon monoxide emissions.[4] As a result, production of MTBE was rapidly accelerated due to the fact that the fuel additive quickly became the most popular fuel oxygenate for achieving the oxygen requirement set forth by the Clean Air Act.[2] Production of MTBE increased steadily from under 1 billion gallons per year in 1982 to over 3 billion gallons per year in 1999. Since 2002, MTBE production has declined.[5] During the 1990's reports of MTBE contamination of ground waters, surface waters, and municipal drinking water supplies within the United States were confirmed.[5] Environmental legislation, ironically, had encouraged rampart production of a highly persistent anthropogenic chemical which subsequently had intimately contaminated the environmental landscape of the United States.

The extent of MTBE contamination of the environment and the potential for detrimental effect on human safety is evident from surveys of public water systems conducted by the Environmental Protection Agency. Public Drinking Water System data ranging from 2000 to 2005 reports concentrations of MTBE above 5 μg/L detection levels in 26 public drinking water systems of some 32,126 systems surveyed. The mean measured MTBE concentration of systems having concentrations above the 5 μg/L threshold was 15.2 μg/L. As compared to other regions, instances of MTBE contamination of public drinking water systems occur at higher frequency in the regions of New England, New York, and New Jersey.[6] A study completed by the National Geological Survey demonstrated that 5% of the public water wells it surveyed had MTBE concentrations greater than 0.2 μg/L. In a separate study, the National Geological Survey also reported that 3% of the unutilized aquifers containing potable water surveyed demonstrated MTBE concentrations higher than 0.2 μg/L.[5] In only three decades time, the prolific fuel economy of the United States was responsible for introducing a new anthropogenic substance to groundwater in detectable quantities throughout the country.

MTBE contamination has been traced to leakage of underground storage tanks on the premises of privately owned gasoline dispensing facilities and industrial sites. In order to better prevent the most probable scenarios for MTBE leakage into the environment from Underground Storage Tanks, the Underground Storage Tank Act mandated that all privately owned Underground Storage Tank systems maintain overfill protection, corrosion control, and leak detection equipment.[7] Recent litigation has led to rigorous enforcement standards for acceptable underground storage. On November 9th, 2006 a $3.1 million USD ruling was ordered by an EPA Administrative Law Judge for the Euclid Company due to 70 violations of statute by underground storage tanks on 23 of the corporation's facilities.[8] While these government actions work to reduce further development of environmental contamination, the current levels of MTBE persistency in American ground and surface waters are sufficient to warrant remediation costs of $2 billion USD as estimated in 2005.[9] These high costs are mandatory to ensure the safety of drinking water sources within the United States.

MTBE destroys potable water due to a distinct odor and taste at minute concentrations. The EPA has placed a warning advisory limit for concentrations above a range of 20-40 μg/L for taste and odor.[10] There is some evidence to suggest that MTBE may be a human carcinogen over prolonged exposures. A four level chronic vapor MTBE exposure study in 1997 monitored the health of Fischer 344 rats over the course of 2 years and reported statistically significant increases in tumors of the kidneys and testes of male rats at the two highest levels of exposure.[1] The major metabolites in the breakdown of MTBE in human liver tissue are tertiary butyl alcohol (TBA) and formaldehyde.[11] Formaldehyde is considered to be a probable carcinogen by the International Association for Cancer Research and the EPA.[2] MTBE groundwater and surface water contamination could very credibly pose a significant risk to human health in addition to degrading the character of potable water resources within the United States.

At point releases of oxygenated fuel, such as surface spillage and underground storage leaks, MTBE is much more mobile than other harmful monitored constituents of oxygenated fuel such as benzene toluene, ethylbenzene, and xylenes (collectively, BTEX). Soil has a very low sorption capacity for MTBE and, due to this fact MTBE travels at a velocity very similar to that of ground water itself under

subsurface porous soil media.[2] In addition to increased mobility as compared to other monitored constituents of fuel spills and leaks, MTBE also is much more resistant to biodegradation. Due to these facts, spills with MTBE content show larger plume sizes than spills that are MTBE free.[2] These characteristics of MTBE lower the performance of conventional containment and passive monitored natural attenuation strategies for the remediation of MTBE point source sites.[12] MTBE is extremely soluble in water over a wide range of concentrations, and has a low Henry's Law Coefficient.[2]

Current available remediation strategies for MTBE groundwater contamination sites can be categorized as either *in situ* methods or pump and treat methods. Both methodologies have a strong dependency on credible data describing the plume size and the evolution of the plume in time.[12] In situ treatments involve containing the plume and treating the contained plume by either air sparging or natural attenuation. These technologies are desirable because they eliminate the expense of pumping groundwater to the surface. In the case of MTBE treatment, the low biodegradation rate and low Henry's Law Constant limit the effectiveness of natural attenuation and air sparging respectively. Air sparging also requires expensive treatment of the air off-gas and is not effective in treating the biodegradation primary breakdown product of MTBE, Tertiary Butyl Alcohol (TBA).[12] Another *in situ* methodology that has been proposed is the permeable reactive barrier process[13]. This strategy involves creating an impermeable barrier in front of the plume path with a permeable gateway filled with treatment catalyst. This methodology is advantageous because it takes advantage of the natural flow of groundwater to drive contact between the feed stream and the catalyst. Activated zeolite ZSM-5 has been suggested as a potential catalyst for the acid catalyzed breakdown of MTBE to TBA and methanol.[13] An appropriate microbial population would be grown at the exit of the gateway to allow microbial degradation of the increased biodegradable catalytic products. The zeolite also has strong adsorption properties for both MTBE and TBA which would allow a slower release of these contaminants to the exit microbial population, favorable to the microbial degradation process of the contaminants. No field data is available, however, to support the viability of this emerging technology in the treatment of MTBE. Pump and treat methods include advanced oxidation, air stripping, and adsorption. Advanced oxidation reactions involve the mineralization of MTBE to carbon dioxide and water. Oxidation proceeds by reaction with hydroxyl radicals which can be generated from the UV reaction of hydrogen peroxide or the reaction of ozone and hydrogen peroxide. These operations require long term storage of hydrogen peroxide, and hydroxyl radicals have preferred reaction kinetics with the BTEX aromatic constituency of petroleum products. Air stripping groundwater pumped to the surface features the same disadvantages as air sparging. A cheap and well demonstrated method of groundwater pump and treat MTBE and TBA remediation is adsorption by a packed tower of granular activated carbon. There is ample field data for the deployment of this technology in treating MTBE leaks and spills.[2] Of the treatment techniques available, packed adsorption towers may be the most inexpensive and practical.

Some of the most effective acceptable remediation techniques, therefore, generally involve adsorption of MTBE into solid phase sorbents.[12] Activated carbon is the most frequently selected sorbent, but silicalite-1 molecular sieve sorbents have been demonstrated to outperform activated carbon by as much as 50,000 μg/g of adsorbent at the low concentrations of MTBE encountered in groundwater remediation applications .[14] Cheap production of hydrophobic molecular sieve adsorbents

for the purposes of removing MTBE from contaminated ground water, could, in conjunction with other emerging technologies, dramatically improve the most recent 2 billion dollar cost estimate for remediation of the natural groundwater and surface waters of the United States.

Zeolite Structure, Nomenclature, and Properties

The classification Zeolite was first appropriated to the naturally occurring $|Na_2\ Ca_8\ (H2O)_{60}|$ **[**$Al_{18}\ Si_{54}\ O_{144}$ **] – STI** crystalline molecular sieve material, stilbite, in 1753 by the Swedish mineralogist Axel Fredrik Cronstedt.[15] The term zeolite translates to "boiling stone", a reflection of the molecular sieve material's propensity for water retention and subsequent heat induced desorption of steam when Cronstedt fused the material in his enlightenment-age blowpipe apparatus.[16] Molecular sieve materials, a much more modern classification, pertain to any crystalline or amorphous porous material with regular pore sizes that can accommodate certain guest molecular species with access to their internal pores while restricting other molecular species, on the basis of their size and shape.[17] Zeolites, in the modern sense, belong to the molecular sieve class of materials, but more specifically, the composition of the zeolite framework, the structure that results in zeolite microporous properties, must be restricted to alumina and silica tetrahedral connected at the vertices.[18] This strict definition allows for a surprisingly rich, wide spectrum of materials with properties required for strong catalytic activity and selectivity in such varied organic reactions as alkane cracking, dewaxing of petrol, and several isomerization and aromatization reactions.[19] The prominent position of zeolite catalysts in the petroleum industry was quickly achieved after the demonstration of the alkane-cracking activity and selectivity improvements over alumina-silica clays in the 1960's and the engineering achievements in zeolite synthesis by Union Carbide and the Mobil corporation shortly thereafter.[19] In addition to revolutionizing catalysis, zeolite materials have also earned a place in various separation processes and ion exchange processes.[16] In the future, engineering process achievements related into growing very large and very small crystals cheaply could begin a new revolution in zeolite utilization in industry and in consumer goods.

The Zeolite framework is composed of tetrahedral basic building units, these units feature a connectivity scheme with central atoms, commonly referred to as T atoms, which are either aluminum or silicon, and four peripheral atoms that are always oxygen.[17] These basic building units may be assembled such that two silicon central atoms or one silicon atom and one aluminum central atom may share a common peripheral oxygen atom, effectively bridging the two basic building units together. Two aluminum atoms, however, are energetically forbidden to form a peripheral bridge, as demonstrated by recent theoretical DFT cluster calculations.[20] Zeolites are tectosilicates, three dimensional anionic networks in which every periphery oxygen atom is shared.[18] Because of the wide range of bond angles permitted by oxygen-silicon-oxygen bonds, 129.1˚ to 180˚, these basic building units have sufficient license to form diverse three dimensional topologies which fall within the zeolite framework classification.[16] Zeolite frameworks can also be seen as made up of intermediate building units, called composite units. These composite units are assemblages of primary units which can be repeated in reoccurring patterns to fully realize periodic zeolite topologies.[18]

Composite building units range from the straightforward double 8-ring unit: two parallel planar eight member rings with the vertices of each ring also connecting orthogonally, to the more complex

three dimensional connectivity of the pentasil unit: eight five member rings connected to one other as to produce an eight faced polyhedron. Such composite building units are named by IUPAC convention by specifying the size of the rings which make up the composite building unit by providing the number of vertices as the base of an exponent, and the number of faces in the unit made up by these rings as an exponent. The smallest rings that make up faces of the unit are listed first, followed by each of the larger rings until each face of the unit is specified.[17] By this convention the double 8-ring unit is named $[4^8 8^2]$ and the pentasil unit is named $[5^8]$.

Composite building units can be used to describe both the framework and pore structures that are characteristic of the zeolite materials. Pores are defined as the polyhedral void spaces that are formed by zeolite framework structures and are the entity that provides zeolites with their molecular sieving character. The faces of the pore polyhedron are called pore windows. Pores that have at least one window large enough to permit entry of a molecule larger than water (a circular window diameter of 2 Angstrom) into the void polyhedral are defined as cavities. Pores that fail to meet the cavity criteria are termed cages. Cavities that extend infinitely in one or more directions are defined as channels. Channels, cavities, and cages can accommodate what are called guest species, molecules and ions small enough to exist within their void polyhedron, while the framework silica and alumina tetrahedron themselves are referred to as the host structure.[17]

It is the chemistry of the zeolite channels, cavities, and cages that define the material's performance with respect to molecular sieving, ion-exchange, and catalytic selectivity.[18] Zeolites with finely tuned channel widths have vast potential with respect to molecular sieving.[19] Sorption performance with respect to separation factor for gases is determined by the ability to selectively adsorb, diffuse, and desorb from either the air swept side of a membrane separator or the recharging stream of a thermal or pressure programmed packed adsorption column.[21] The most important property of these channels is their smallest pore dimension in the direction orthogonal to the direction of their infinite channel extension, termed the effective channel width.[17] Channels are not truly infinitely extended, but instead their lengths are related to the macroscopic zeolite crystal size. Larger crystal sizes also can provide enhanced selectivity for catalysis and separation applications. Larger crystals provide longer regular channels which may offer preferred diffusion kinetics for certain guest species. Due to this fact, large crystals are desirable in achieving greater catalytic selectivity in many organic reactions by allowing preferred products, which do not vary appreciably in size, to be separated from other products on the basis of their polarity. Ultimately, zeolite pore properties dictate the materials performance in molecular separations.

In addition to the geometry of pore windows, the chemical identity of the T atoms that make up a pore window influences the properties of zeolite materials. Alumina tetrahedron, an aluminum (III) T-atom with four oxygen periphery atoms, have an overall of charge (-1) while silica tetrahedron, a silicon (IV) T-atom with four oxygen periphery atoms, have an overall neutral charge. Thus, alumina bridged to silica gives pore windows a charge imbalance feature which is normally alleviated by the presence of a mobile extra-framework monovalent guest cation localized within the pore.[18] These localized extra-framework cations are defined as compensating cations, and it is their chemistry that dictates the performance of zeolite materials in ion-exchange processes.[18] Hydrogen proton compensating cations

are localized in a quasi-bond with the bridging peripheral oxygen atom between the silicon and aluminum atoms, effectively creating bridging hydroxyl groups in the zeolite pore window.[22] It is this strong Brönsted acid site provided by these structures that catalyze SN1 type organic reaction mechanisms such as alkane cracking[19]. The localized nature of these acidic sites, within the zeolite pore, make zeolite SN1 catalytic mechanisms pronouncedly selective by restricting access to the active sites to guest species larger than the intended reactants or products. The chemistry and geometry of zeolite frameworks make them invaluable to petrochemical industry.

Zeolite frameworks can be synthesized with wide stoichiometric variations of alumina content. The silicon to aluminum ratio within typical zeolite frameworks can range from 1 to arbitrarily large. Alumina content is important in altering the properties of zeolite pores providing for higher catalytic activities or providing preferred diffusivities for either polar or non-polar guest species.[19] The presence of aluminum in a pore window leads to more active sites for organic SN1 reaction mechanisms, however a high density of alumina sites leads to more prominent poisoning of the sites and lower macroscopic acidity due to the diminishing electro negativity of the framework, thus decreasing catalytic activity[23]. With respect to sorption properties, sufficient alumina content leads to increasingly polar electric character of the windows of the channels that make up a zeolite pore network due to the charge imbalance each alumina site contributes. These increasingly polar channels are highly hydrophilic, while, in contrast, dealuminated channels are highly hydrophobic, offering preferential diffusion kinetics to organic guest species that are large and electrically neutral.[19] Water molecules are readily loaded into pore spaces of a wide variety of zeolites, but dealuminated species are relatively water free.[18] Alumina content is a microstructure feature of zeolite frameworks that may be widely varied and leads to profound effects on zeolite properties.

Any given state of a zeolite material may be named according to IUPAC rules. The smallest repeating volume element of the periodic crystal, the unit cell, provides all of the information necessary for complete identification and characterization of a crystal structure and can be used to create a model of any arbitrary morphology. According to convention, the zeolite is named by the stoichiometry of its defect-free unit cell. First, the stoichiometry of the guest species occupying the unit cell are given in straight brackets, followed by the stoichiometry of the framework atoms given in bold square brackets, followed by a dash and the three letter code of the zeolite framework in bold. The three letter codes for zeolite frameworks are abbreviations for the well known common names appropriated to each particular framework. Silicalite-1 has the IUPAC designation:

[$Si_{80}\ O_{144}$**]** $_h${3[5^8]}$_p${1[10]<100>(0.54)/1[10]<010>(.56)}**-MFI**.

According to nomenclature conventions recommended for IUPAC, this name describes, in addition to the stoichiometry of the unit cell, that the host may be constructed from only the pentasil composite unit, and that the structure has two channel networks. The first channel extends indefinitely in one crystallographic dimension, is composed of a double 10 ring composite unit ([10]) extending in the <100> crystallographic direction and has an effective width of 0.54 nm. The second pore has a width of 0.56 nm and also extends in one direction, the <010> direction, and is built from the 10 member composite unit. The channel in the <100> traverses a sinusoidal path, while the wider channel in the <010> is a

straight path channel**.** Silicalite-1 and ZSM-5, an aluminated MFI structure zeolite, both usually display coffin-shaped crystal morphology. The crystal is typically longest in the <001> crystallographic direction. The figure below demonstrates silicalite-1 and ZSM-5 crystal morphology and the microstructure of their pores. Zeolites, in general are defined by their guest species, alumina content of their frameworks, and geometry of their pores.[17]

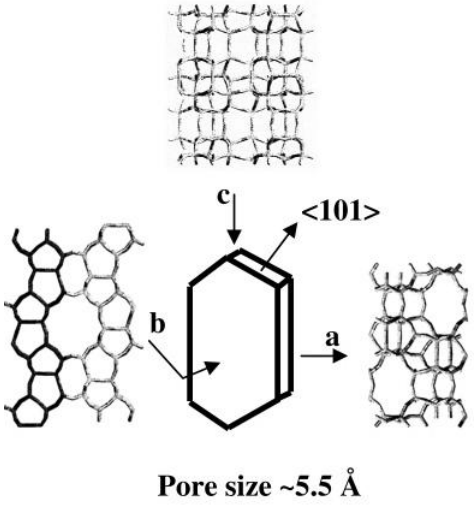

Figure 1: MFI pore structure and crystal habit

Zeolite states can be tuned with respect to alumina content and pore geometries at the time of synthesis by applying engineering principles to established synthesis techniques. The all-important properties of the zeolite materials currently available are limited only by the ability of synthesis techniques to develop cheap, uniform, sustainable varied microstructure production processes.

Zeolite Synthesis

Synthetic preparation of zeolite materials began in earnest in the late 1940's based on the pioneering work of R.M. Barrer. He was able to demonstrate that zeolite frameworks could be synthesized cheaply and easily with simple laboratory equipment.[24] In 1948, Robert M. Milton's group at Union Carbide Corporation initiated research into zeolite production, building on the work of Barrer, and as a result of their efforts, Union Carbide Corporation entered the zeolite market in 1954. Since that time, Union Carbide Corporation, the Mobil Corporation and independent researchers have combined to develop over 80 synthetic frameworks.[25] New frameworks continue to be developed in modern zeolite synthesis research, such as the recent mesoporous frameworks developed by the Mobil Corporation in 1996[19], although much modern zeolite synthesis research concerns itself with control of the crystal morphologies of established synthetic frameworks.

In spite of the wide variety of microporous crystal structures that can be synthesized, virtually all zeolite synthesis procedures share the same features. An aqua-gel solution is created within caustic media containing a silica source, an aluminum source when applicable, and a structure directing agent when applicable. The structure directing agent is a non-framework organic base which participates in

complex interactions with zeolite precursors. These interactions influence the progression of zeolite crystal growth sufficiently to direct the building novel frameworks.[26] The aqua-gel, containing the charge of nutrients necessary for zeolite synthesis, is sealed in a vessel and exposed to elevated temperatures (usually between 60 °C-180 °C) in a batch process. The solubility of the gel phase is higher than the solubility of the newly formed zeolite phase and so the resulting equilibrium between the amorphous gel phase, supersaturated aqueous phase, and newly formed zeolite crystal phase at high temperature and autogenous pressure provides the driving force for zeolite homogenous nucleation. Under these same conditions, subsequent crystal growth of formed nuclei competes with continued nucleation until all nutrients are depleted and the batch synthesis is stopped. Due to the variety of parameters involved in the crystallization phenomenon batch times can vary from hours to days.[27] For batches that include a structure directing agent, the organic base will be trapped within the pores of the zeolite at the time synthesis is stopped. In that case, the resultant as-synthesized zeolite must be calcined—exposed to temperatures between 450-550 °C for 2-3 hours, in order to destroy the organic base within the pores, restoring the useful properties of the zeolite.

A number of different silica sources can be used for hydrothermal synthesis. For this purpose, colloidal silica, sodium silicate, or tetra ethyl ortho silicate (TEOS) is acceptable. Aluminum can be introduced into the aqua-gel from sources such as aluminum hydroxide, alumina, or sodium aluminate. Structure directing agents vary depending on the framework which is to be synthesized. Other parameters which can be varied to produce different zeolite frameworks and crystal sizes are the silica to aluminum ratio, the water content, the pH, and the presence of any cations in solution. These parameters have a strong influence on not only the identity of the framework which is synthesized, but also on the crystal size distribution, the yield of solids, and the crystallinity of the yielded solids.

Current zeolite synthesis research is dominated by the need to grow very large or small crystals of existing zeolite frameworks, as opposed to the development of new frameworks. A wide variety of applications exist for crystals at the extremes of the crystal size spectrum. Instances of batch produced macroscopic particles of crystal aggregates are desirable for large scale chemical separation processes and catalysis processes. There is sufficient demand for batch synthesis processes that are affordable and can tightly control the final morphology and crystal sizes of the aggregates of these materials, such as the process demonstrated in this work.

Fixed Bed Adsorption Columns

Macroscopic zeolite packing could be extremely useful in developing a fixed bed adsorption process for wastewater treatment of MTBE. Most current adsorption columns for these applications feature a fixed loading of packing of granular activated carbon (GAC) within a cylindrical column commonly composed of lined carbon steel.[28] Typical adsorption columns are 7-10 ft in diameter and 20-40 ft tall. The lining may be selected to suit the corrosion and abrasion resistance required for the wastewater application considered. Wastewater feed is most often delivered to the bottom of the column and effluent is collected from the top to minimize head loss. Over the lifetime of operation the column packing will become saturated with adsorbed contaminant and regeneration of the packing is required. Regeneration is usually accomplished thermally by delivering the saturated packing to a multi

hearth furnace by screw conveying. Furnaces containing rotating rabble arms and are usually natural gas fired. Regenerated, reactivated carbon can then be redelivered to the column and another treatment cycle may take place. Adsorption columns packed with granular activated carbon are an established technology that has obtained acceptable target treatment concentrations in municipal and industrial settings since the 1970's.

The wastewater feed in intimate contact with the solid packing allows for the mass transfer of contaminant from the aqueous phase to the solid adsorbent phase by sorption phenomenon. If the packing has extended surface area due to a microporous framework such as silicalite-1, the contaminant is of a sufficiently small molecular size, and diffusion kinetics are sufficiently fast, diffusion into the extended internal surface area will provide dramatically higher sorption capacities as compared to non porous packing. The breakthrough curve for a particular adsorption process is the plot of effluent concentration over time. It is a direct measure of the lifetime of the adsorption process before regeneration of the packing is in order. In a bottom to top liquid delivery adsorber configuration, saturation of adsorbent occurs first at the bottom of the packing and then proceeds to the top. The effective continuous volume of mass transfer, the mass transfer zone, decreases while the saturated zone increases. At the time that the effective zone of mass transfer reaches the top of the column, an inflection point occurs in the breakthrough curve. After this point of inflection, the breakpoint, the effluent concentration increases rapidly to another inflection point, the exhaustion point, at which all driving force for mass transfer is extinguished and the concentration more slowly reaches the feed concentration. The S- shaped curve that results determines the lifetime of the adsorbent process before the recharging operation must occur.

It follows that column packing that could outperform activated carbon could lead to less instances of the expensive thermal regeneration step. Furthermore, the use of zeolite packing to adsorb MTBE, could lead to the utilization of an advanced oxidation regeneration procedure[29] instead of the overly expensive thermal regeneration step. Less iterations of the thermal regeneration procedure or substitution with chemical regeneration would lead to natural gas savings as well as less operation of the scrubber located downstream of the furnace flue gas. Silicalite-1 zeolite, or dealuminated ZSM-5, is a zeolite species which is comprised of the MFI, or Mobil Five framework. Due to the fact that it has no alumina in the framework, silicalite-1 is hydrophobic and is an excellent candidate for a fixed bed MTBE adsorbent. As noted already in this work, silicalite-1 was shown to outperform activated carbon in this role in laboratory experiments by adsorbing as much as 50,000 μg/g adsorbent more than activated carbon at low concentrations of MTBE .[14] In order to realize full scale utilization of these laboratory findings, however, a variety of scale-up engineering problems must be resolved.

In order for useful implementation of silicalite-1 packing for adsorption column applications to be realized, synthesis methods must be developed to produce packing on the order of millimeters as opposed to the powder form that it is traditionally available. A typical large scale commercial activated carbon adsorption columns features a pressure drop across the bed of 35 psi with an inlet pressure of 60 psi[28]. The pressure drop across a theoretical bed can be calculated by the Ergun equation:

$$f_p = \frac{150}{Re_p} + 1.75$$ Equation [1]

$$f_p = \frac{\Delta p}{L}\frac{D_p}{\rho V_s^2}\left(\frac{\epsilon^3}{1-\epsilon}\right)$$ Equation [2]

$$Re_p = \frac{D_p V_s \rho}{(1-\epsilon)\mu}$$ Equation [3]

The largest silicalite-1 zeolite powders have crystal sizes of 120 µm, this would lead to a pressure drop of 2000 psi for a column of 10 diameter and 20 ft height with typical hydraulic particle loading. Increasing the particle size, by aggregating the crystals into spherical packing of 3 mm diameter would reduce the pressure drop to 20 psi, making the technology feasible. For silicalite-1 packing to be a viable alternative to activated carbon packing, the packing must approach a 3 mm particle size. It is for this reason that the subsequent laboratory scale investigation into the development of large spherical aggregates of silicalite-1 micro crystals has been undertaken.

II. EXPERIMENTAL

Reagents:

Silica Gel Beads:

Silica gel beads sold by EM Industries for use as a desiccant under the trade name t.h.e.™ ("the highly efficient desiccant") were used as the starting source of silica material for each synthesis conducted. The gel particles have a reported value of 4 mesh particle size. Experimental investigations conducted during this work revealed an average particle size of 3.1 cm diameter, a particle weight of 0.190 g, and each particle adsorbed 37% of the particle weight in water before becoming saturated.

Structure Directing Agent:

Tetrapropylammonium Bromide salt obtained from Aldrich Chemical Company (Catalog number: 22 556-8), or 40% by weight Tetrapropylammonium hydroxide (TPAOH) solution obtained from Johnson Matthey (Lot number: K08B04) was used as the structure directing agent in each of the synthesis experiments conducted.

Other Reagents:

A summary of all of the reagents used in this work are provided in Table 1.

Table 1: List of Reagents

Reagent:	**Obtained from:**
Ludox AS-40 Colloidal Silica	Aldrich
Sodium Silicate (Na_2SiO_3*$5H_2O$), granular	EM Industries
Sodium Hydroxide (NaOH), pellets (97%)	Aldrich
Nitric Acid (HNO_3), 60% by weight solution	Aldrich
Ammonium Hydroxide (NH_4OH), 30% by weight solution	Aldrich
Triple exchanged and triple filtered purified water	Barnstead Nanopure II

Laboratory Equipment:

All experiments were conducted in sealed 8 mL, 1.5 cm diameter Teflon-lined stainless steel, Morey-type autoclaves. For the synthesis experiments conducted using the steam assisted conversion method, the autoclave was modified to include a stainless steel 6-mesh tray to support ten beads above 2 mL of water. Autoclaves were cleaned after each experiment with a warm solution of nitric acid under a fume hood.

To minimize breakage of the hydrophilic silica gel beads when immersed in aqueous solution, care was taken to saturate each bead with water content before introduction to hydrothermal solutions. Saturation of the beads was accomplished by modifying an 8 L desiccator to suspend 500 beads above

2L of water. A curved glass condensation shield was included above the bead plate to protect the beads from any liquid contact when gentle heating (100 ^{o}C) was applied to the bottom of the desiccator.

All experiments were heated in an automatic controlled convection oven. The weight of all component reagents of the hydrothermal solutions, as well as the weight of the starting beads and the finished product beads, was measured by an OHAUS Explorer™ laboratory balance last serviced on 6/22/09 by Precision Laboratory Corp. A 1 horsepower, 2750 rpm vacuum pump drove the vacuum filtration process utilized in the washing of beads after the hydrothermal treatment step. Each bead was calcined in a muffle furnace at 550 °C for two hours after the hydrothermal treatment step.

Analytical Equipment:

X-ray diffraction experiments were performed with a Geiger-Flex 2 diffractometer and a Cu K_{α} x-ray tube. A goniometer step size of .1° and dwell time of 1 second were maintained for all experiments. Each bead was ground into a fine powder with a mortar and pestle before being placed on a glass sample holder for diffraction experiments. Crystallization scores were assigned to each batch based on the ratio of the area of the large peak found at 23° 2-theta to that of a ZSM-5 powder sample obtained from ZEOCHEM.

Scanning electron microscopy was accomplished with an AMRAY-2 microscope. All pictures featured in this work were taken by electrons generated under a potential difference of 15 kilovolts and a stable emission current of 55 micro amps. Each bead was stabilized on a brass mounting peg with dried carbon paint and sputter-coated at a current of 45 mA for 75 s with a gold-palladium alloy to ensure conductivity of the sample. Crystal sizes were assigned by the length of the largest crystal dimension. For the typical coffin-like crystal habit of silicalite-1 this dimension is the [001] crystallographic direction.

Vicker's Hardness Testing was accomplished by use a Vicker's hardness test apparatus. Beads were first mounted on a fast hardening epoxy resin to stabilize the beads during indentation, polished and indented to provide hardness ratings on the Vicker's hardness scale.

Zeolite Synthesis Batch Recipes:

A number of different batch recipes were prepared over the course of this work. The following table summarizes these procedures.

Table 2: Recipes for Silicalite-1 Batch Synthesis

The Steam Assisted Conversion Method without Excess Silica

Composition of Hydrothermal Solution:			
Reagent:	*Weight (grams)*	*Moles*	*Mole Fraction*
Tetrapropylammonium Hydroxide	10.8	0.053	0.056
Water:	16.2	0.899	0.944
Temperature (°C):	180		
Ratio of Silica to Structure Directing Agent within the Bead:	22.87		

The Steam Assisted Conversion Method with Excess Sodium Silicate

Composition of Hydrothermal Solution:			
Reagent:	*Weight (grams)*	*Moles*	*Mole Fraction*
Tetrapropylammonium Hydroxide	6.8	0.033	0.055
Sodium Silicate:	2.15	0.010	0.017
Water:	10.2	0.566	0.928
Temperature (°C):	180		
Ratio of Silica to Structure Directing Agent within the Bead:	26.06		

The Steam Assisted Conversion Method with Excess Colloidal Silica

Composition of Hydrothermal Solution:			
Reagent:	*Weight (grams)*	*Moles*	*Mole Fraction*
Tetrapropylammonium Bromide:	6.44	0.032	0.010
Colloidal Silica:	10.88	0.181	0.059
Ammonium Hydroxide:	8.46	0.241	0.056
Water:	46.86	2.60	0.851
Temperature (°C):	180		
Ratio of Silica to Structure Directing Agent within the Bead:	108.9		

Hydrothermal Treatment of Silica Gel Beads

Composition of Hydrothermal Solution:			
Reagent:	*Weight (grams)*	*Moles*	*Mole Fraction*
Tetrapropylammonium Bromide:	5.505	0.021	0.007361908
Sodium Hydroxide:	0.492	0.012	0.004380038
Water:	50	2.77	0.988258054
Temperature (°C)	137 to 180		
Ratio of Silica to Structure Directing Agent within the Bead:	121.8		

Synthesis Procedure:

In each synthesis procedure, 10 cured beads were selected for each batch. The particle size of each bead was measured with the assistance of digital photography prior to any contact with the hydrothermal solution. The hydrothermal solution or each batch was prepared by blending reagents in the proportions enumerated in Table 2. In the case of the steam assisted conversion method, all of the beads from simultaneous batches were first immersed in 30mL of the solution for 24 hours in a 150 mL sealed polypropylene bottle prior to being sorted into units of 10, mounted as a unit above 2 mL of water in each autoclave, and heated. In the case of the hydrothermal method, beads were simply placed in the autoclave with 5 mL of hydrothermal solution, sealed, and pre-aged for 24 hours before heating.

Autoclaves were placed in a convection oven for varied durations of time. After removal from the oven, each autoclave was rapidly quenched in a cold water bath before opening. Beads were then removed from the autoclaves, washed with water over a vacuum filtration system, and placed in clay crucibles for the calcining process. Calcining was achieved at 550°C for two hours in a muffle furnace. After the calcining process, product particle sizes and weights were recorded and analytical characterization experiments were conducted on the beads.

III. RESULTS AND DISCUSSION

The conversion of silica gel beads to zeolite aggregate particles is achieved by complex hydrothermal mechanisms and because the particle size distribution within the bead cannot be tracked *in situ* as the synthesis proceeds, careful measurements before and after the hydrothermal steps, intuition, and logical rationalization are relied upon in understanding and improving the process. The steam-assisted conversion methodology is a viable pathway to low cost production of silicalite-1 packing suitable for full scale fixed bed adsorption columns, only if the process is carefully controlled such that crystallization is halted by rapid quenching before the approximate last 0.008 cubic centimeters of amorphous silica, located at the center of the bead is converted. If complete conversion of amorphous silica occurs, the resulting mechanical properties of the bead are too poor for successful scaled up utility in a packed fixed bed adsorption column. The amount of amorphous silica at the core of the bead can be carefully tuned by the operator to strike a balance between more favorable adsorption performance and more favorable mechanical properties. Tuning the amorphous content of the finished product requires knowledge of the crystallization vs. time curves of the system, careful control of the starting particle sizes of amorphous silica batch feed, and knowledge of the radial concentration profile of structure directing agent within the beads at the start of exposure to elevated hydrothermal temperature.

Structure directing agent within the bead must be considerably higher than concentrations typical to bulk solution hydrothermal synthesis due to the large silica reservoir provided by the amorphous silica gel housing the aqueous solvent within its macroscopic pores. The pores vary from 5 Angstrom to 3000 Angstrom in width and, with a large enough nutrient population of structure directing agent available, are suitable localizations for silicalite-1 nucleation and crystal growth mechanisms. As the large feed stock of amorphous silica available to crystallization mechanisms is converted to a dense regular periodic phase, the higher density of the crystal phase leads to warping of the original shape of the silica bead. As amorphous silica at the radial coordinates of the bead closest to the surface begin to undergo crystallization mechanisms before more central coordinates of the bead, it drives silica and structure directing agent nutrients from central starting locations into the developing crystal phase, which quickly evolves into a shell of densely inter-grown crystal aggregates. Below is an SEM photograph of this shell of crystal aggregates at a magnification of 30X, as well as a photograph of the morphology of the aggregated crystals at 4000X.

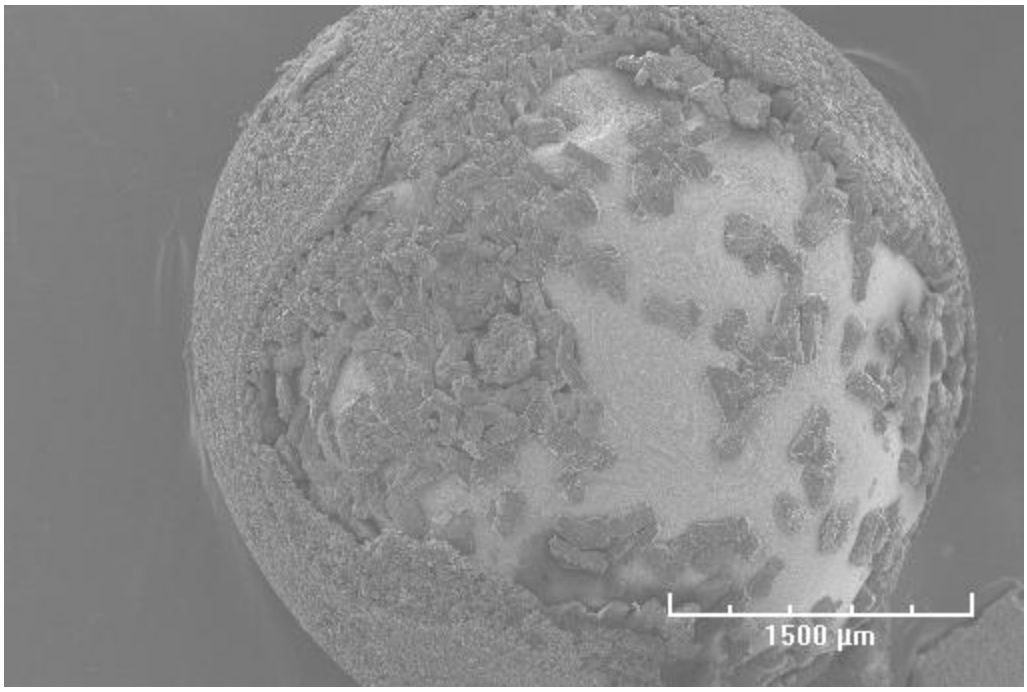

Figure 2: Silicalite-1 crystal aggregate shell with incomplete surface coverage at 30X magnification

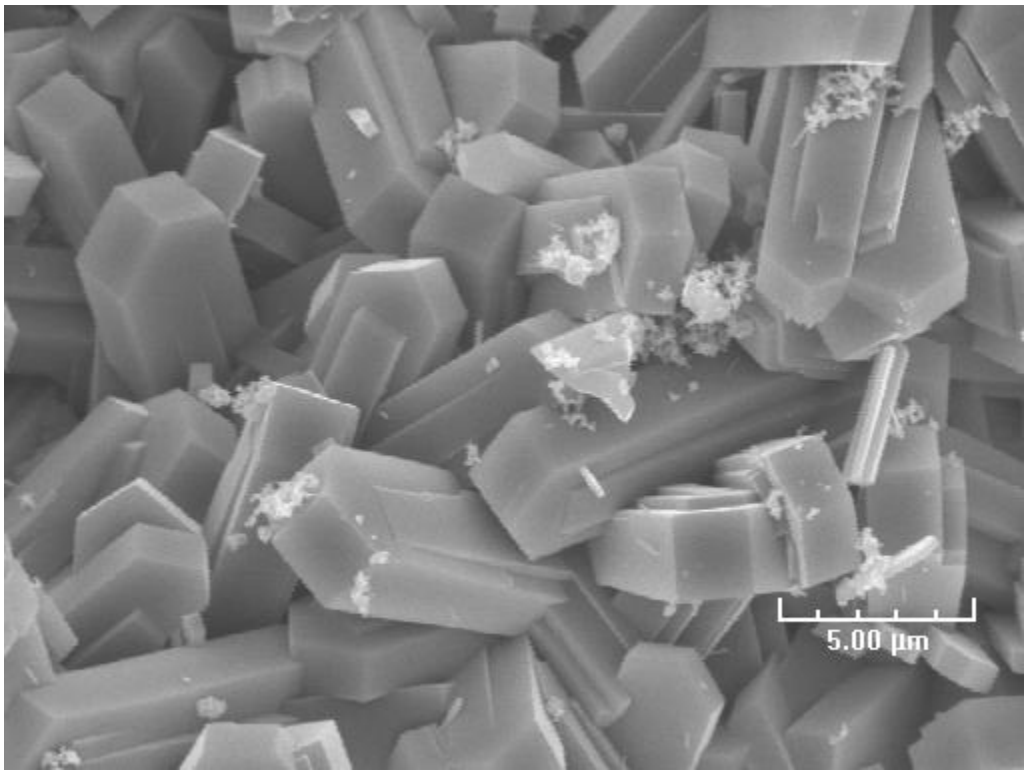

Figure 3: Silicalite-1 crystal aggregates at 4000X magnification

The process eventually depletes the central core of the original bead of nutrients until all structure directing agent becomes incorporated into the crystal aggregate phase or all amorphous silica is converted to silicalite-1 crystals. In the event that ample structure directing agent is available, the densification of the original amorphous gel bead results in a void space at the core of the macroscopic bead and unacceptably low yield strength of the product. Controlling the amount of structure directing agent initially charged into the bead before the batch steam assisted hydrothermal treatment step of the packing production process is engaged may be the cheapest approach to effectively controlling the conversion of the amorphous bead to maximize yield strength of the product.

Understanding the crystal curves, or the plot of crystallization vs. time, for the silicalite-1 hydrothermal treatment system is essential in controlling the conversion of amorphous silica for each batch. The following curve summarizes the crystallization score of several hydrothermal synthesis experiments performed by immersing 2g of hydrated silica beads in a hydrothermal solution following recipe 4 and cooking for several days in a convection oven at 137°C and at autogenous pressures.

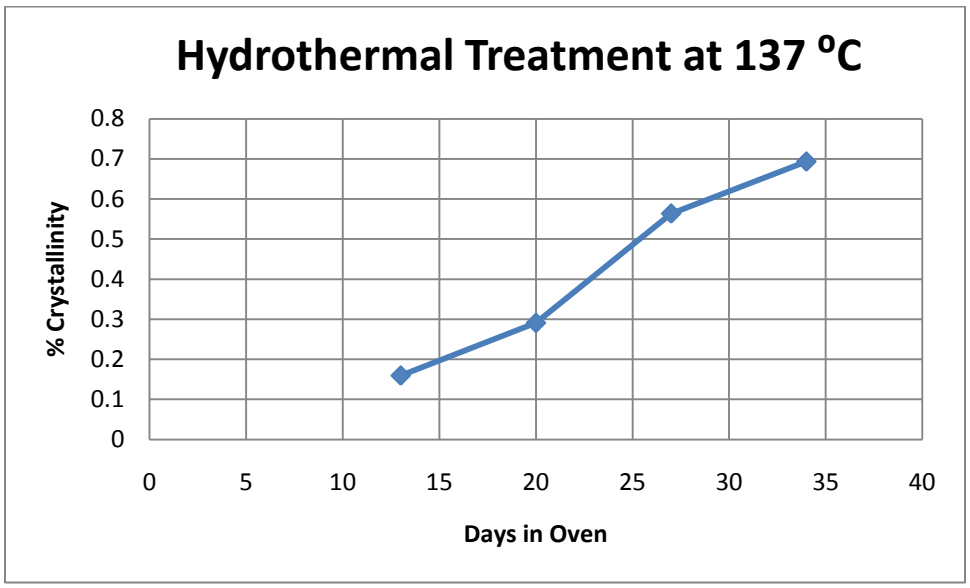

Figure 4: Low temperature crystal curve for silicalite-1

Appreciable crystallization proceeds extremely slowly. Cleavage of the finished, calcined beads revealed that the region of dense 30 micrometer crystal aggregates takes place only as a shell around the amorphous silica substrate. Only after prolonged periods of time does the shell grow in thickness.

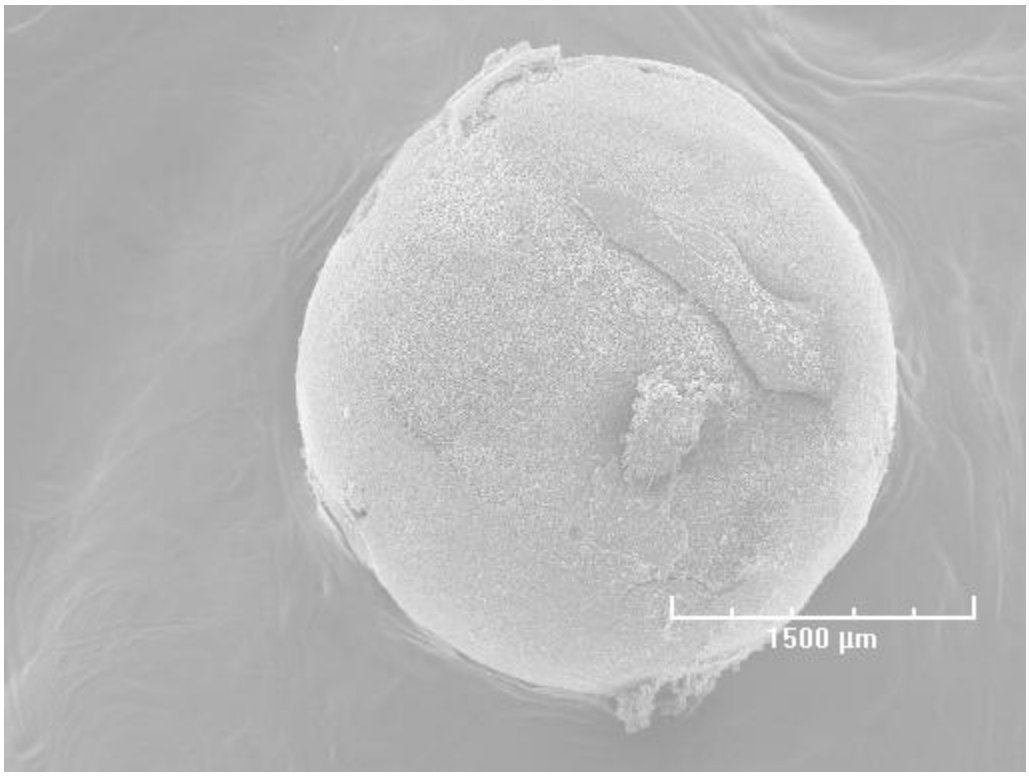

Figure 5: Bead with a shell of silicalite-1 aggregates covering the surface

Naturally, increasing the temperature of the hydrothermal synthesis step decreases the time for appreciable crystallization. Rather than directly proceeding to 180 °C, the maximum available temperature for operations in TEFLON™ lined autoclaves, experiments were conducted at a smaller temperature adjustment to 150°C to ensure that increased temperature did not have a detrimental effect on the quality of the product. A second crystallization curve summarizes the benefit of operating the batch process at 150°C.

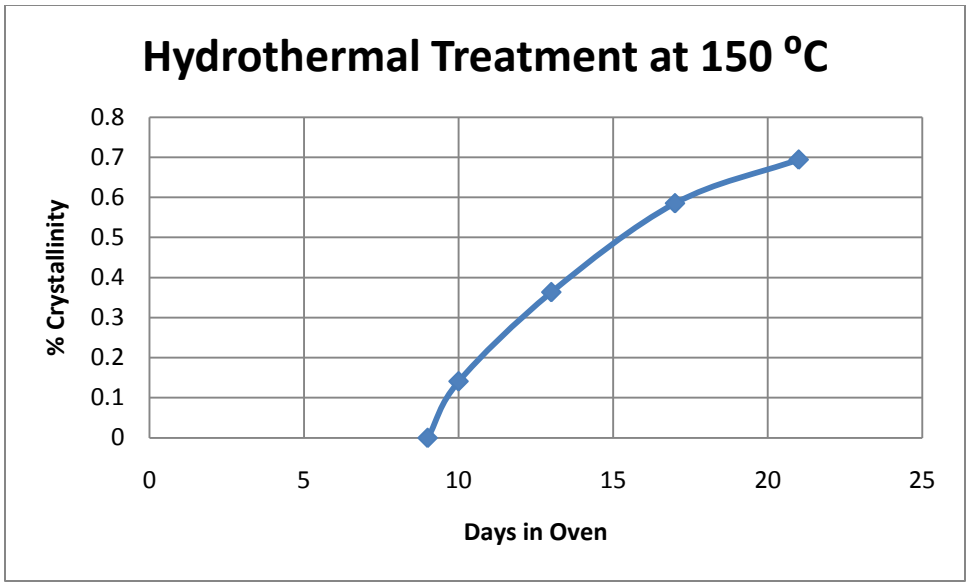

Figure 6: Intermediate temperature crystal curve for silicalite-1

The resultant silicalite-1 aggregate shell x-ray diffraction patterns were indistinguishable from those obtained in the previous experiment, but the process was considerably faster than the low temperature experiments.

The experiments conducted at 180 °C, summarized in the table below, show aberrant crystal habit as evidenced from the x-ray diffraction experiments, also shown below.

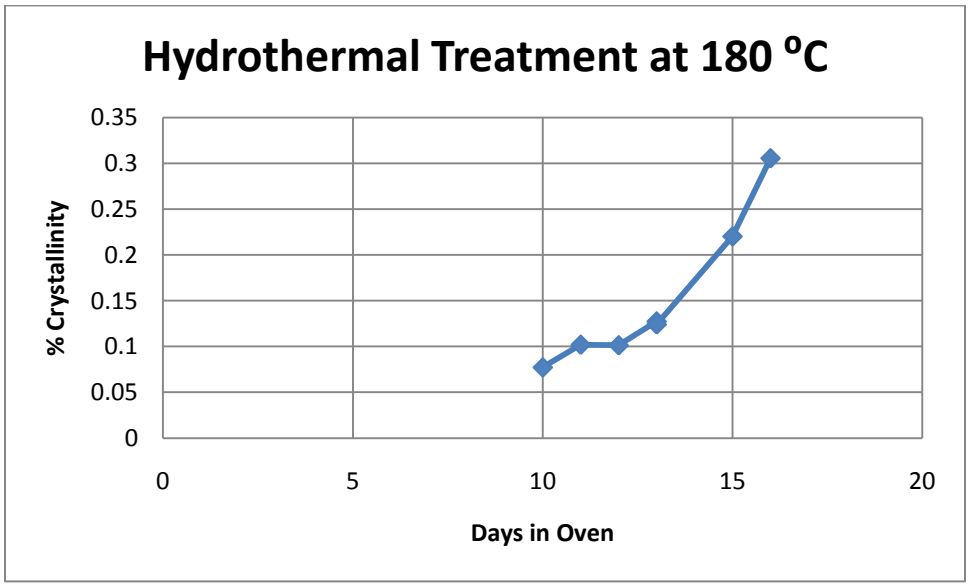

Figure 7: High temperature crystal curve for silicalite-1

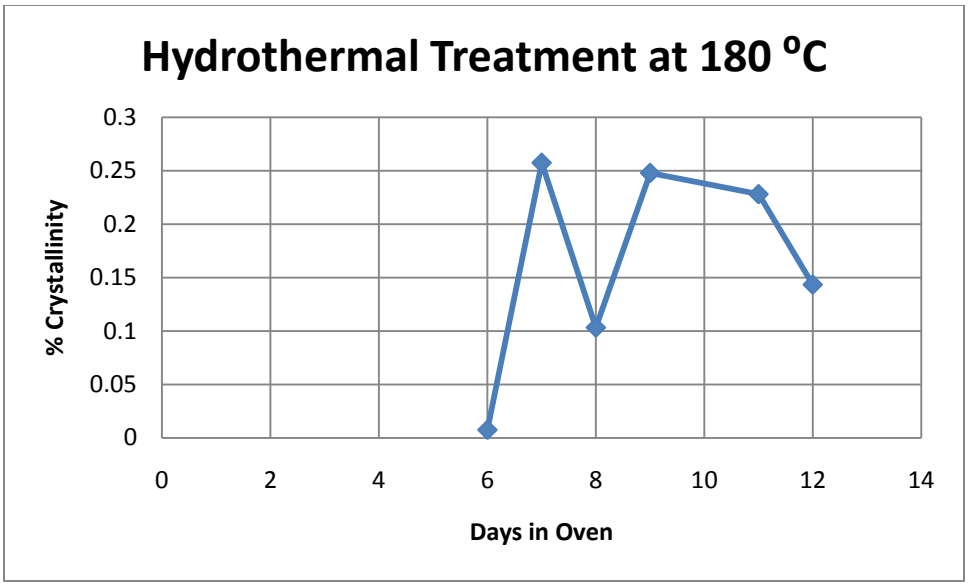

Figure 8: High Temperature silicalite-1 crystal curve additional data set

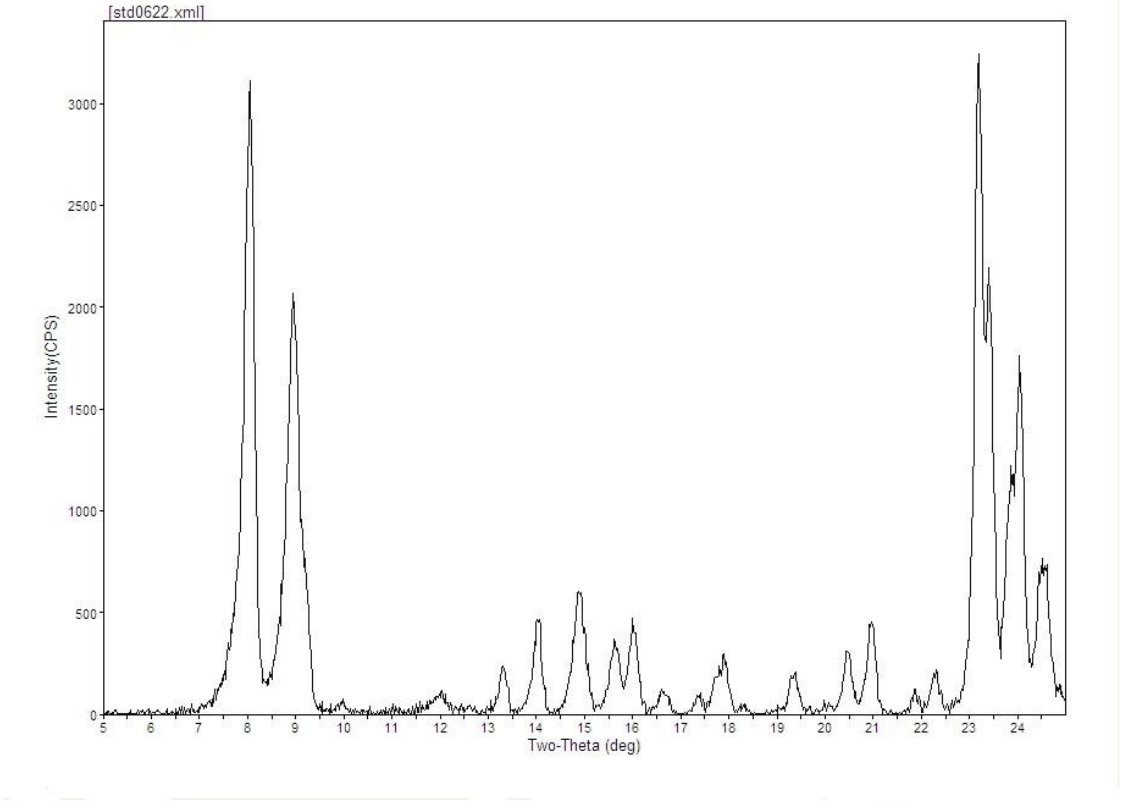

Figure 9: Typical silicalite-1 morphology x-ray powder diffraction pattern

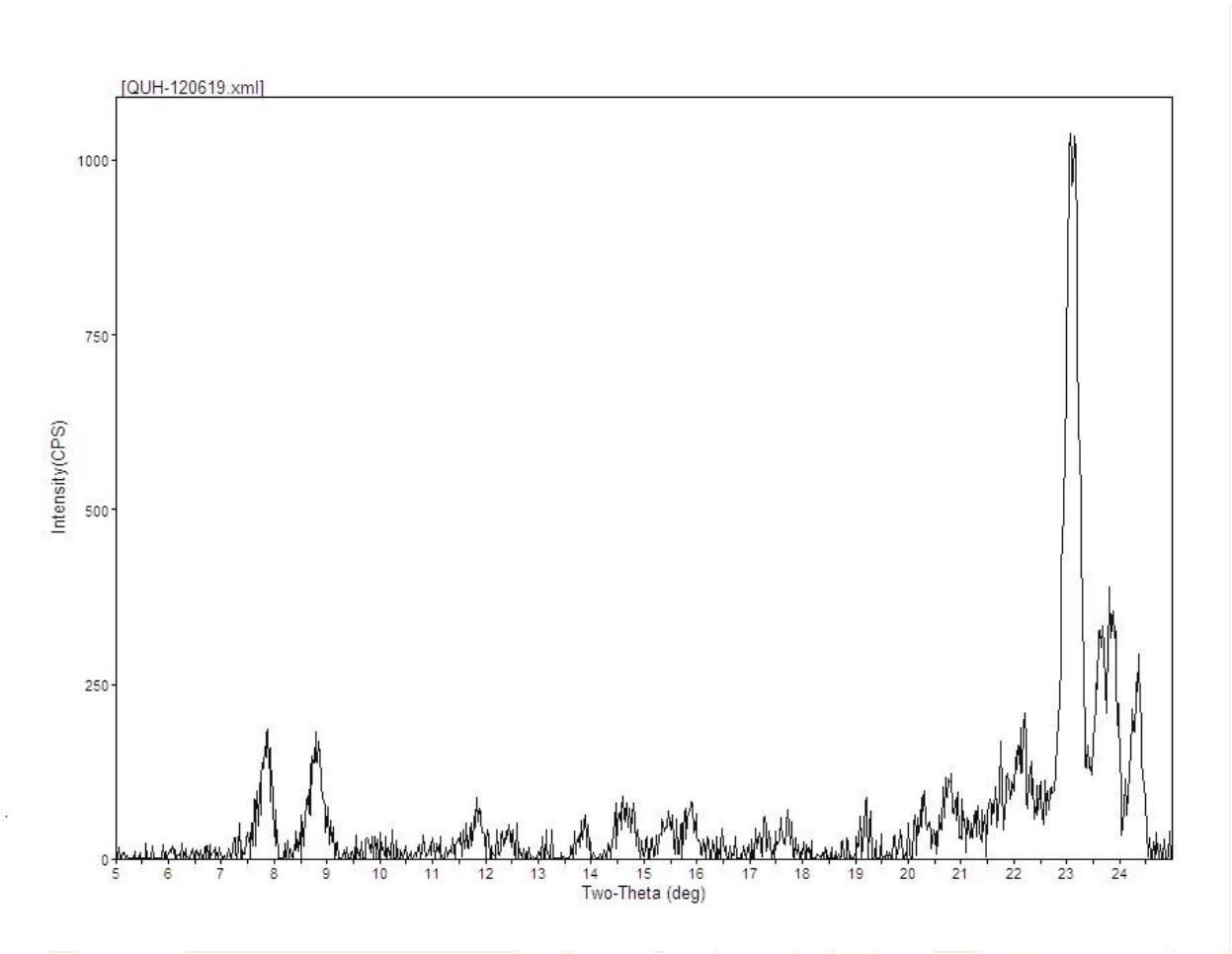

Figure 10: Silicalite-1 x-ray diffraction pattern of a high temperature experiment demonstrating preferred orientations

The striking feature when comparing these two x-ray diffraction patterns are the much lower intensities of the peaks located at 8 and 9 degrees two-theta with respect to the intensity of the peak at 23 degrees two theta. The first two peaks are caused by the (200) and (020) faces of the silicalite-1 crystal habit[30] and the high temperature pattern suggests an appreciable difference in habit shape and aspect ratio as compared to the lower temperature crystal morphologies.

Further investigation of this phenomenon by SEM microscopy of a finished batch from the earliest stages of the high temperature crystallization curve reveals that instead of a typical coffin-like morphology, crystals nucleated and grown at this particular temperature demonstrate a more rounded leaf-like morphology.

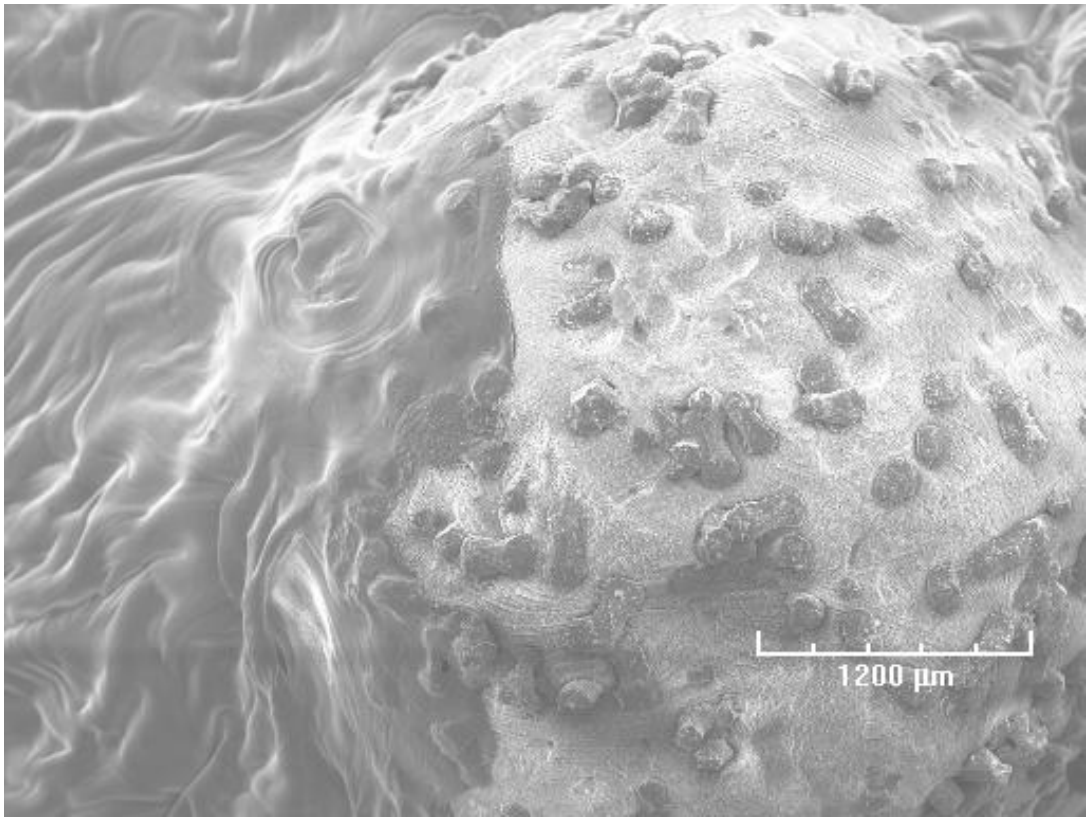

Figure 11: High Temperature Crystal Morphology

The crystal morphology suggests a hindering effect that takes place during nucleation resulting in the absence of the alternating (101) and $(\bar{1}01)$ terminations that produce the coffin-like crystal faces seen in typical morphology as the crystals grows, as suggested by Isabel Diaz and coworkers in their work done synthesizing silicalite-1 with different structure directing agents.[31] This higher temperature effect may be more of a structure directing agent concentration effect, due to increased convective transport of structure directing agent due to larger temperature gradients as transient heat transfer equilibrates within the bead during the initial stages of nucleation. Nuclei born of this unusual morphology due to high concentrations of structure directing agent at birth, could in turn influence the morphology of subsequent nuclei born from the autocatalytic nucleation mechanism. Supporting this assertion is the fact that these morphologies are observed in all of the high temperature and high structure directing agent synthesis experiments conducted after this experiment.

It appears that all of the experiments discussed so far have in common the fact that structure directing agent is the limiting reagent. Crystallization proceeds slowly and eventually plateaus, leaving a somewhat desirable amorphous silica gel core at the center of the bead with minimal void space separating the shell from the core. Further experimentation was conducted at higher initial charge concentrations of TPAOH within the amorphous feed material. In these experiments, the beads, charged with a aqueous solution of 40% by weight TPAOH, were suspended in the autoclave on a mesh

support above a 2mL level of water to ensure that the beads did not dry up over the course of the conversion at high temperature. These experiments were conducted again at the highest temperature permitted for autoclave operations, but the most interesting point from these experiments is the evolution of the radial temperature profile inside the bead, rather than the oven temperature.

The charging of the batch process, the exposure of the feed amorphous silica beads to the TPAOH solution for 24 hours, leaves the beads with more or less a uniform concentration profile of structure directing agent. Under ideal heat transfer conditions, this uniform concentration profile could be heated concentration-gradient-free to temperatures sufficiently high for silicalite-1 nucleation mechanisms to take place. If these facts were true, a single nucleation event would take place within the same time frame resulting in the subsequent growth of equally-sized crystals simultaneously within the pores of the amorphous silica. The end result would be a uniform bead of aggregated crystals and distributed void space. Because these conditions could not be satisfied with useful feed particle sizes of amorphous silica, the mechanical strength of such a particle remains a mystery.

The high thermal resistivity of amorphous silica instead dictates that crystallization in this batch process initiates at the edge of the sphere and proceeds in the inward radial direction. For incompressible flows within mesoporous materials, the non-linear Navier-Stokes equation is coupled with the enthalpy balance in a somewhat complex way due to the dependency of viscosity on temperature.[32] The end result is the temperature-gradient-driven convection of TPAOH from positions near the center of the bead to outer surface of the bead as the transient heat transfer process of bringing all of the radial position of the bead into equilibrium proceeds sufficiently slowly. When the conditions become appropriate for nucleation at the surface of the bead, these same conditions are still developing near the center of the bead, because of the deficiency of structure directing agent at this location. As crystallization proceeds, a much stronger driving force to more fully deplete the center zone of structure directing agent develops in the form of the densification of the amorphous silica; concentration gradients rapidly develop as a result. If, however, the batch process is halted before complete conversion results, the product beads have mechanical properties suitable for their intended application, as packed bed adsorbents.

Stopping the batch just before complete conversion of amorphous silica takes place in the excess of structure directing agent requires strict control of feed particle sizes. Larger particles alter the heat transfer characteristics that are important in deciding the thickness of the first crystal aggregate zone that develops on the outer surface of the bead. Naturally, due to the additional mass included with a larger particle of silica gel, larger beads take longer to reach complete conversion. In spite of having to carefully measure particle sizes, the benefit of operating with an excess of structure directing agent is dramatically faster crystallization curves. Below is a summary of the operating conditions and crystallization curves for a synthesis procedure that made use of recipe 1.

Table 3: Low Silica:TPAOH experiments

Hydrothermal Treatment Time (hours)	Mean diameter of feed particles (cm)	Std dev. of feed particle diameter	Mean dry bead weight (g)	Crystallinity of product
5.37	3.90	0.024	0.037	0.325
6.75	4.01	0.036	0.039	0.015
6.9	3.87	0.028	0.038	0.767
7.5	3.73	0.031	0.038	0.322
7.88	3.94	0.023	0.039	0.031
8.5	3.62	0.029	0.041	0.315
9	3.90	0.018	0.042	0.513

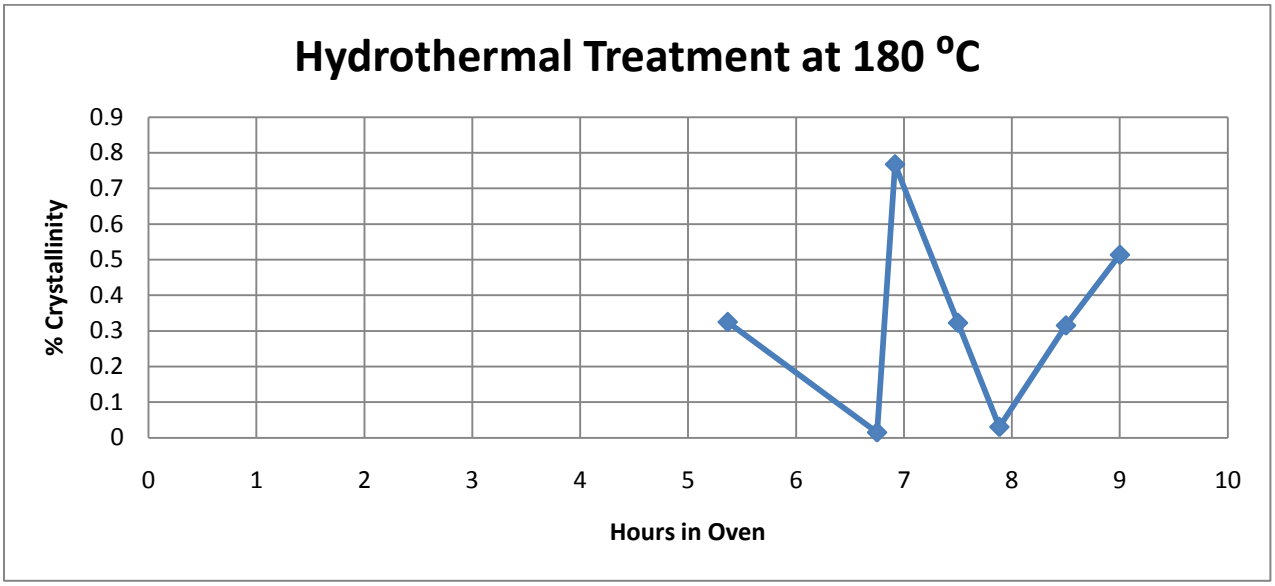

Figure 12: Low Silica:TPAOH crystallization curve

While there is strong variability in the output product crystallization, this crystal curve demonstrates that in the present of excess structure directing agent, crystallization proceeds decidedly faster: high crystallinities can be achieved in seven hours as opposed to several days. However, in spite of the controlled feed particle sizes, there is much variance with respect to how much crystallization takes place within each bead in the batch.

The following table summarizes crystallization measurements observed over different cooking times and also within the same batch under a SEM. Included are some pictures of the shell and core structures of the finished beads, and the measurements of the geometry of these structures as obtained from SPIRIT SEM imaging software pixel counts. The average crystal size is the average of the longest

spatial dimension of each sampled crystal found in the aggregation zone. The void percent is the ratio of the diameter of the amorphous core to the diameter of the aggregate zone minus twice the thickness.

Table 4: Comparison of geometrical parameters of silica gel conversion features

Hours heated at 180 °C	Feed mean diameter (cm)	Std dev of feed diameter	Average Crystal Size(µm)	Diameter of aggregate zone (µm)	Thickness of aggregate zone (µm)	Void percent
31	2.85	0.052	4.34	3557	143	0.99
8	3.15	0.038	7.5	4158	67	0.99
8	3.18	0.039	3.06	3510	216	0.83
8	3.18	0.039	8.25	3636	162	0.88
8	3.2	0.027	11	3718	78	0.92
8.5	3.62	0.029	23.95	4244	105	0.85
8.5	3.62	0.029	21.46	3982	142	0.93
7.5	3.73	0.031	20.69	3342	138	0.99
7.5	3.73	0.031	7.272	3838	186	0.99
6.92	3.87	0.028	19.67	4048	163	0.97
9	3.9	0.018	13.8	3954	415	0.75
9	3.9	0.018	27.6	4048	653	0.99
7.88	3.94	0.023	24.5	4410	121	0.91
7.88	3.94	0.023	23.4	3965	40	0.99
6.75	4.01	0.036	20.72	4049	270	0.93

Of note is the fact that while the thickness of the aggregate zone varies widely, the diameter of the aggregated zone remains more or less the same between experiments. This evidence supports the assumption that crystallization first takes place at the outer surface of the sphere and that subsequent nucleation and growth take place in the inward direction towards the center of the bead. The observation of void space confirms that when conversion is complete the finished product will be a hollow sphere. This fact cannot be experimentally confirmed, because the completely converted spheres are too brittle to be accurately cleaved and examined.

Some SEM pictures are included to depict the crystallization phenomenon and how the geometric attributes of the crystal shell and amorphous core were determined. The SEM pictures of the crystalline aggregate zone shell demonstrate decreasing crystal sizes from the surface of the sphere in the direction of decreasing radial coordinate from the center. Again this evidence supports the assertion that the front of the nucleation activity gradually moves towards the center as crystallization proceeds.

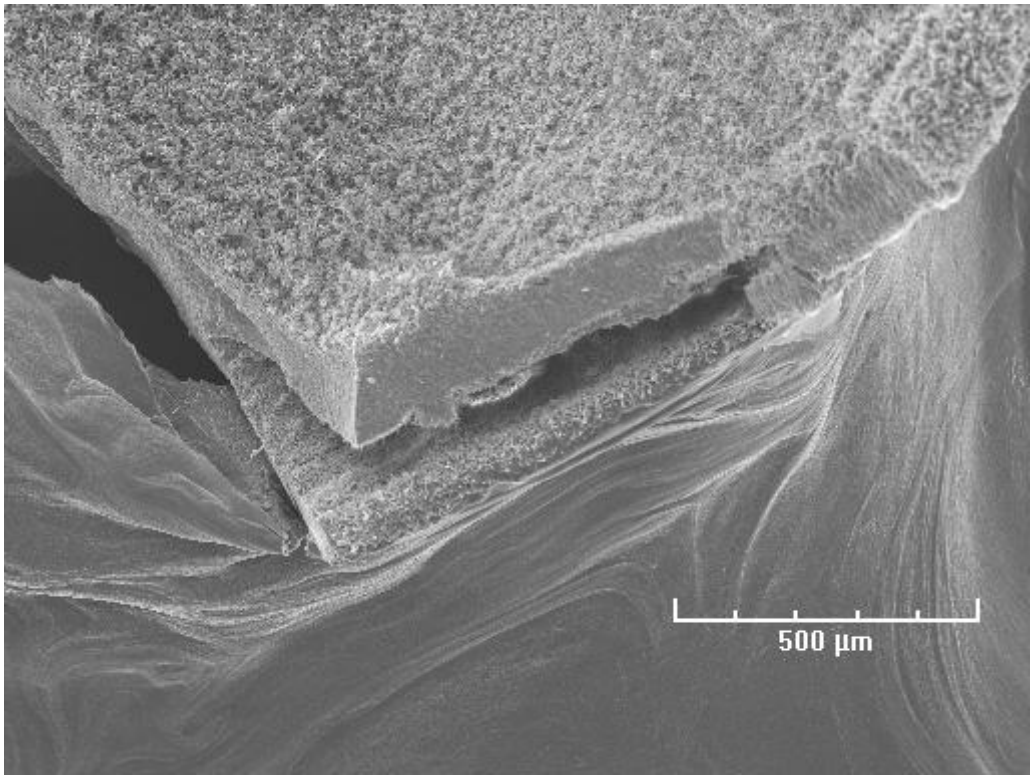

Figure 13: The silicalite-1 aggregate shell at low magnification

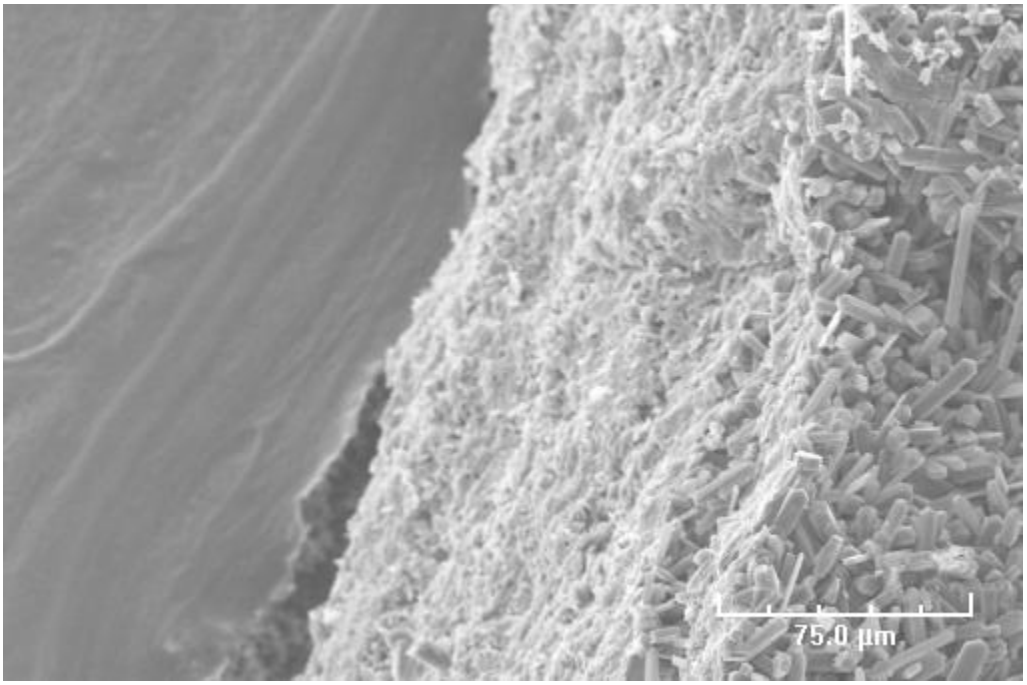

Figure 14: The silicalite-1 aggregate shell at 500X

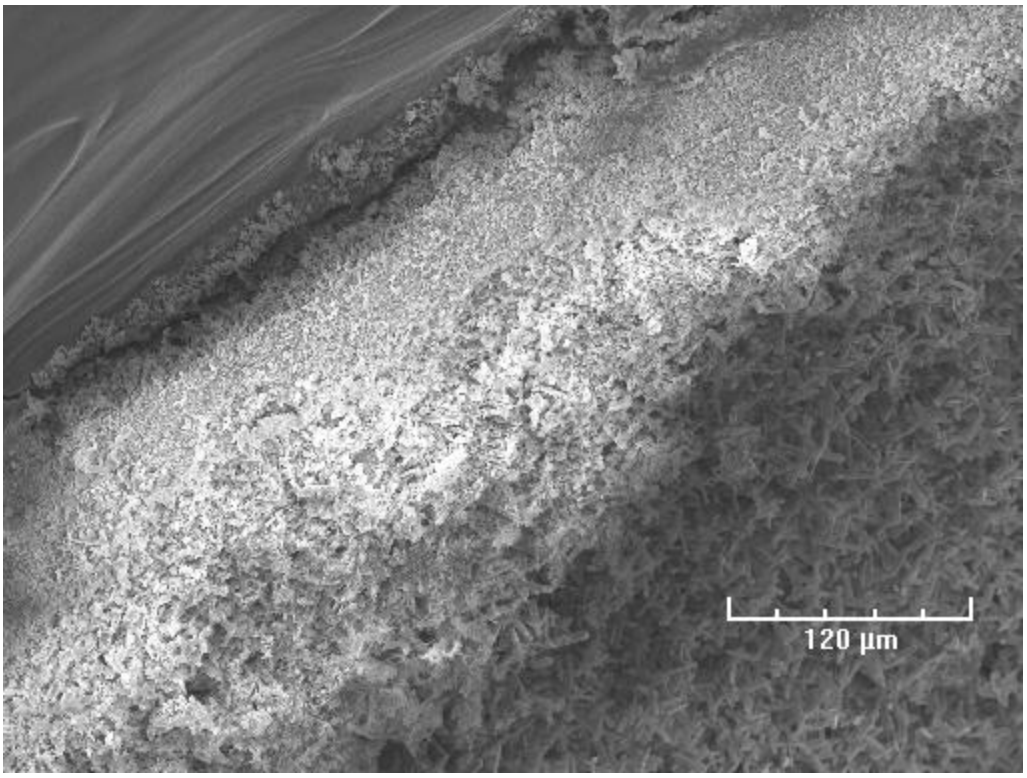

Figure 15: The silicalite-1 shell demonstrating thickness and curvature

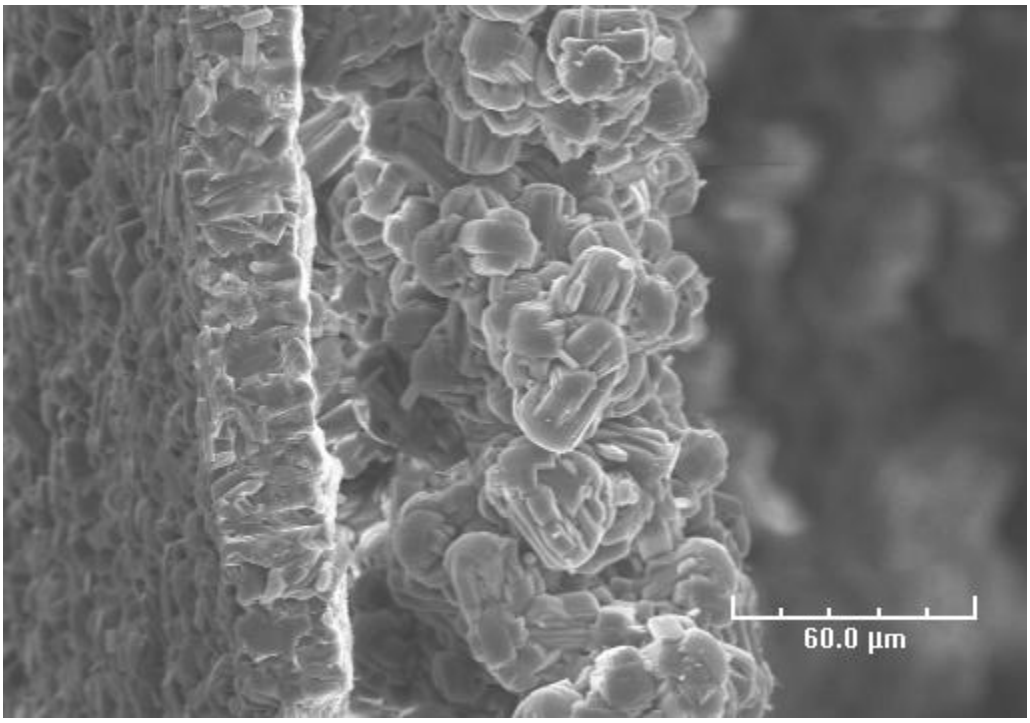

Figure 16: A silicalite-1 shell with small crystal sizes and leaf-like morphology of aggregates

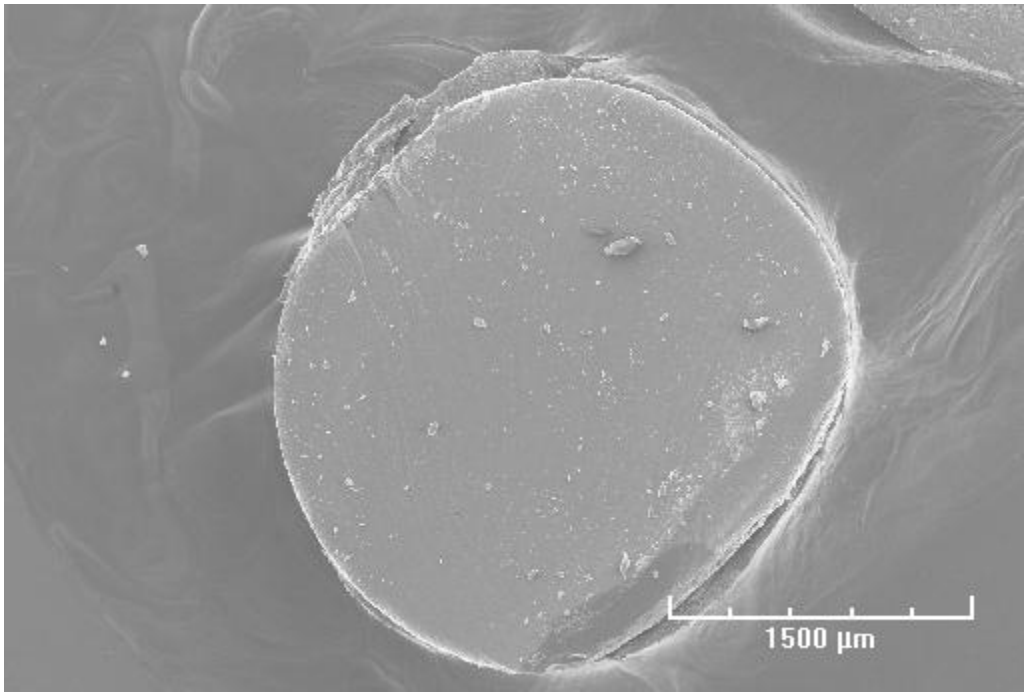

Figure 17: The amorphous core within the incompletely converted sphere, cleaved in half to demonstrate the absence of crystallization within

As an alternative to timing the synthesis to retain an amorphous core, excess silica could theoretically be charged into the bead to allow complete retention of the shape of the sphere as densification proceeds. The amount of silica that can be charged into the bead in conjunction with the requisite high concentration of structure directing agent is constrained by solubility limits. The high concentration of TPAOH required for the experiments undertaken in this study were at the solubility threshold. As Raoult's law implies, very little solubility is available for dissolved silica. In spite of this fact, a three-level experiment was performed by preparing in random order 4 experiments at each of three treatment levels of dissolved sodium silicate added to the solution. The three levels were the addition of 1.6%, 3.2%, and 4.8% excess silica to the batch in the form of sodium silicate. Such low percentages of the total silica content of the batch were selected to minimize upset of the silica:TPAOH ratio that had been found to be successful in promoting fast nucleation and growth of silicalite-1. The results of a Levene's test for homoscedasticity, and the subsequent ANOVA f-test to test the hypothesis that the mean of all three populations are equal is included below. Either because there is too much inherent variance in the process to make a strong distinction between treatments; because the 12 hour time scale chosen was not a long enough time for any of the excess silica to be converted; or because the same equal small amount of dissolved sodium silicate was able to reach the pores during the charging process in all three treatments, changing the amount of sodium silicate did not seem to have an appreciable effect.

Lavene's Test	
2	Degrees of freedom between treatments
9	Degrees of freedom within treatments
W Statistic:	0.51193
critical f for (5% , 2, 9):	3.065

Table 5: Hypothesis testing performed on 3 level treatment experiments

RAW DATA	Group	Score:
Sample1	2	0.9712198
Sample2	2	0.346427829
Sample3	1	0.010919301
Sample4	3	1.665401414
Sample5	2	0.377859817
Sample6	1	0.329658902
Sample7	1	0.932846298
Sample8	3	1.226185524
Sample9	2	2.616940516
Sample10	3	0.777142263
Sample11	1	0.826305116
Sample12	3	0.409629784

Hypothesis Testing:

Treatment:	Mid	Low	High
	0.3464278	1.665401414	0.0109193
	0.3778598	0.409629784	0.8263051
	2.6169405	0.777142263	0.9328463
	0.9712198	1.226185524	0.3296589
Group Mean:	1.078112	0.950724487	0.5249324
Overall Mean:	0.8512563		
SSw Calculation:			
	0.5353617	**0.51076311**	**0.2642095**
	0.4903531	**0.292783478**	**0.0908255**
	2.3679932	**0.030130788**	**0.1663937**
	0.0114259		**0.0381317**

SSt Calculation:			
		0.662832273	0.7061663
	0.2548518	0.195033976	0.0006226
	0.2241042	0.00549289	0.0066569
	3.1176408		0.2720638
	0.0143913		

ANOVA TABLE	SS	DOF	MSS
SS between Treatments:	0.6614849	2	0.3307425
SS within Treatments:	4.7983718	9	0.5331524
SS Total for all Treatments:	5.4598568	11	

f statistic:	0.6203526
critical f for (5% , 2, 9):	3.065

Hypothesis:	μ1=μ2=μ3
Failed to Reject the Null Hypothesis	

The mechanical properties of the silicalite-1 packing were investigated in the form of a Vicker's hardness test performed on a wide range of aggregate crystal sizes. The following chart summarizes the results.

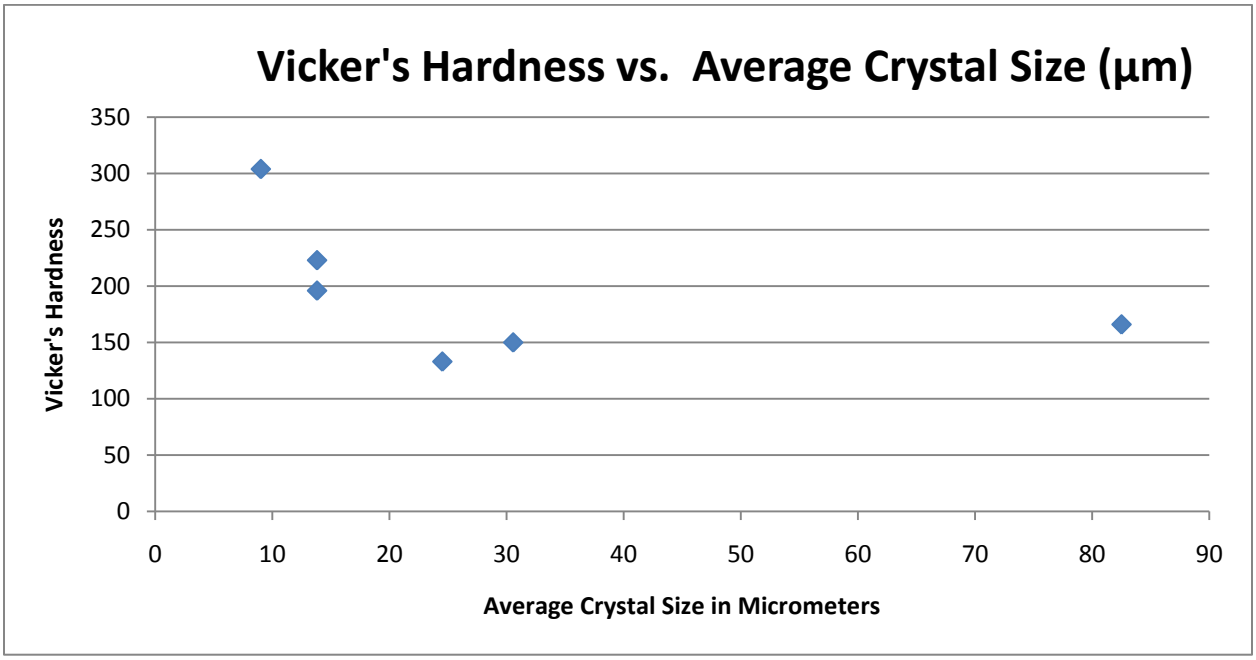

Figure 18: Vicker's Hardness testing of various crystal sizes of synthesized silicalite-1 aggregate packing spheres

As expected, smaller crystal aggregates demonstrate increased micro-hardness and greater resistance to micro-fracture. These results suggest that finished aggregate beads with small crystal sizes and sufficient amorphous mass at the center should be suitable for use in packed column applications. Typical Vicker's hardness test values are 140 for 316L stainless steel and 12 for quartz. Cylindrical wafers created from grinding natural zeolite into grain sizes of 100µm, pressing into wafers at 100 MPa after agglomerating with polyvinyl alcohol, and thermally treating at 1150 °C were reported to have a Vicker's hardness value of 80.[33] The aggregates tested in this work appear to be substantially harder than those natural zeolite aggregates. However, the Vicker's hardness testing values reported here are not extremely accurate due to the small size of the depressions as well as the fact that there was little visual contrast between the aggregate sample and the mounting epoxy. Due to this fact, the measurements best serve as a demonstration of the increasing relative hardness that can be achieved by lowering the average crystal size of the aggregates. In spite of the admittedly low accuracy of the testing, the fact that none of the samples were measured as having a Vicker's hardness value lower than 100 is suggestive that they are sufficiently strong to be utilized in a packed column application.

IV. CONCLUSIONS

Complete conversion of amorphous silica into silicalite-1 packing particles with shape retention has been demonstrated to be possible, but particles synthesized by this methodology suffer from such poor mechanical properties that they are unusable in packed bed installations. However, fine tuning of the amount of unconverted amorphous silica located at the center of the bead when synthesis is halted before complete conversion takes place leads to silicalite-1 packing that should have sufficient properties to permit their use as adsorbent packing for the groundwater and surface water treatment of MTBE at leak and spill sites. It may be possible to create silicalite-1 particles without appreciable void space and with sufficiently small crystal sizes that allow a packing composed solely of silicalite-1 material to withstand the demands of packed column applications. However charging the beads simultaneously with the necessary silica content and structure directing agent for this approach to be feasible is an engineering obstacle that must first be overcome.

V. FUTURE WORK

The next step in development of this particular technology is conducting pilot scale experimentation with the silicalite-1 aggregate packing. Breakthrough curves are required at this scale. The results of pilot scale testing may lead to the need for more laboratory scale development experimentation.

The robustness of this procedure for obtaining other aggregates of useful molecular sieve materials should be investigated. Creating aggregates of ZSM-5 pellets which could subsequently be activated would be invaluable in a wide range of applications.

Incorporation of iron into the pores could lead to a one step destruction of MTBE by catalyzing an advanced oxidation reaction within the zeolite pellet. This technology could be implemented in pump and treat fixed bed, but due to the low oxygen content in groundwater, the attractive alternative, in situ advanced oxidation, would not be effective without air sparging, which would lead to further complications.

This process needs further development before being ready for commercial operation, but it is a cheap process that has potential in the treatment of difficult to separate organic contaminants in wastewater.

VI. REFERENCES

1. M.G. Bird, H. D. B.-F., J.S. Chun, J.F. Douglas, J.J. Kneiss, and L.S. Andrews, Oncogenicity Studis of Inhaled Methyl Tertiary-butyl Ether (MTBE) in CD-1 Mice and F-344 Rats. *Journal of Applied Toxicology* **1997,** 17, (7), S45-S55.
2. David J. Kortum, L. H., Loren Beard, Kim Liechty, Mark Coryell, and Chris Bruner, Interagency Assessment of Oxygenated Fuels. In Council, N. S. a. T., Ed. 1997.
3. Piel, W. J. In *Historical Perspective on the Use of Ethers in Fuels*, Conference on MTBE and Other Oxygenates, Fairview Park Marriott, Falls Church, Virginia, July 26, 1993, 1993; Fairview Park Marriott, Falls Church, Virginia, 1993.
4. The Clean Air Act. In *42*, 1955; Vol. 7545, p 270.
5. John S. Zogorski, J. M. C., Tamara Ivahnenko, Wayne W. Lapham, Michael J. Moran, Barbara L. Rowe, Paul J. Squillace, and Patricia L. Toccalino *Volatile organic compounds in the Nation's ground water and drinking-water supply wells*; U.S. Geological Survey: 2006, 2006.
6. Agency, U. S. E. P., UCMR1 List 1 and List 2 Chemical Monitoring Data. In.
7. Solid Waste Disposal Act. In *42*, 1976; Vol. 6991-6991b, pp 133-141.
8. U.S. Environmental Protection Agency *v*. Euclid of Virginia, Inc. In 2006; pp 2-3.
9. Frank Sweet, M. K., Tabatha Pellerin, David Espy, and Michael Mills, An Estimate of the National Cost for Remediation of MTBE Releases from Existing Leaking Underground Storage Tank Sites. In Agency, E. P., Ed. ENSR International Corporation: 2005.
10. Agency, U. S. E. P., Drinking Water Advisory: Consumer Acceptability Advice and Health Effects Analysis on Methyl Tertriary-Butyl Ether. In 1997.
11. Wolfgang Dekant, U. B., Elisabeth Rosner, Alexander Amberg, Toxicokinetics of ethers used as fuel oxygenates. *Toxicology Letters* **2001,** 124, 37-45.
12. ITRC, Overview of Groundwater Remediation Technologies for MTBE and TBA. In Interstate Technology & Regulartory Council: 2005.
13. Centi, G.; Perathoner, S., Remediation of water contamination using catalytic technologies. *Apllied Catalysis B: Environmental* **2003,** 41, 15-20.
14. Ayşe Erdem-Şenatalar, J. A. B., Arjan Giaya, and Robert W. Thompson, Adorption of Methyl Tertiary Butyl Ether on Hydrophobic Molecular Sieves. *Environmental Engineering Science* **2004,** 21, (6), 722-729.
15. Colella, C.; Gualtieri, A. F., Cronstedt's zeolite. *Microporous and Mesoporous Materials* **2007,** 105, 213-221.
16. Barrer, R. M., *Hydrothermal Chemistry of Zeolites*. Academic Press Inc.: New York, 1982.
17. McCusker, L. B.; Liebau, F.; Engelhardt, G., Nomenclature of structural and compositional characteristics of ordered microporous and mesoporous materials with inorganic hosts. *Pure Apllied Chemistry* **2001,** 73, (2), 381-394.
18. Barrer, R. M., *Zeolite and Clay Minerals as Sorbents and Molecular Sieves*. Academic Press Inc.: New York, 1978.
19. Thomas, J. M. T. a. W. J., *Principles and Practice of Heterogeneous Catalysis*. VCH Verlagsgesellschaft mbH: Weinheim, Federal Republic of Germany, 1997.
20. Limtrakal, J.; Tantanak, D., Cationic structural and compositional effects on the surface structure of zeolite alumino silicate catalysts. *Chemical Physics* **1996,** 208, 331-340.
21. Seader, J. D.; Henley, E. J., *Seperation Process Principles*. John Wiley & Sons, Inc.: New York, 1998.
22. Uytterhoeven, J. B.; Christner, L. G.; Hall, W. K., Studies of the Hydrogen Held by Solids. VIII. The Decationated Zeolites. *The Journal of Physical Chemistry* **1965,** 69, 2117-2126.
23. Tielers, F.; Langenaeker, W.; Geerlings, P., Ab initio study of the bridging hydroxyl acidity and stability in the 12-membered ring of zeolites. *Journal of Molecular Structure* **2000,** 496, 153-162.

24. Rees, L. V. C. Richard Maling Barrer, FRS. http://www.iza-online.org/RMBarrer.htm (December 15, 2009),
25. International Zeolite Association. http://www.iza-online.org (January 5, 2010),
26. Moor, P.-P. d.; Beelen, T. P. M.; Santen, R. A. v.; Beck, L. W.; Davis, M. E., Si-MFI Crystallization usinga "Dimer" and "Trimer" of TPA Studied with Small-Angle X-ray Scattering. *Journal of Physical Chemistry B* **2000,** 104, 7600-7611.
27. Thompson, R. W., Recent Advances in the Understanding of Zeolite Synthesis. In *Molecular Sieves Science and Technology: Synthesis*, Karge, H. G.; Weitkamp, J., Eds. Spriger-Verlag: Berlin, 1998; Vol. 1, pp 1-33.
28. Cheremisinoff, P. N.; Ellerbusch, F., *Carbon Adsorption Handbook*. Ann Arbor Science Publishers Inc.: Ann Arbor, 1978.
29. Koryabkina, N.; Bergendahl, J. A.; Thompson, R. W., Adsorption of disinfection by products on hydrophobic zeolite with regeneration by advanced oxidation. *Microporous and Mesoporous Materials* **2007,** 104, 77-82.
30. Yu, H.; Wang, X.-q.; Long, Y.-c., Synthesis of b-axis oriented high silica MFI type zeolite crystals introduced with co-template role. *Microporous and Mesoporous Materials* **2006,** 95, 234-240.
31. Diaz, I.; Kokkoli, E.; Terasaki, O.; Tsapatsis, M., Surface structure of zeolite (MFI) crystals. *Chem. Mater.* **2004,** 16, (25), 5226-5232.
32. Hessel, V.; Hardt, S.; Lowe, H., *Chemical Micro Process Engineering*. Wiley-VCH: Weinheim, 2004.
33. Hernandez-Velez, M.; Raymond-Herrera, O.; Alvardado-Martin, A.; Jacas-Rodriguez, A.; Roque-Malherbe, R., New materials obtained from high temperature phase transformations of natural zeolites. *Journal of Material Science Letters* **1995,** 14, 1653-1656.